Molecular and nanostructural mechanisms of deformation, strength and toughness of spider silk fibrils

Andrea Nova[1,2], Sinan Keten[1], Nicola Pugno[1,3], Alberto Redaelli[2], Markus J. Buehler[1,3,4,5†]

[1] *Laboratory for Atomistic and Molecular Mechanics, Department of Civil and Environmental Engineering, Massachusetts Institute of Technology, 77 Massachusetts Ave. Room 1-235A&B, Cambridge, Massachusetts 02139, USA*

[2] *Dept. of Bioengineering, Politecnico di Milano, P.zza Leonardo da Vinci 32, 20133, Milano, Italy*

[3] *Dept. of Structural Engineering and Geotechnics, Politecnico di Torino, Corso Duca degli Abruzzi 24, 10129, Torino, Italy*

[4] *Center for Materials Science and Engineering, Massachusetts Institute of Technology, 77 Massachusetts Ave., Cambridge, Massachusetts 02139, USA*

[5] *Center for Computational Engineering, Massachusetts Institute of Technology, 77 Massachusetts Ave., Cambridge, Massachusetts 02139, USA*

[†] Corresponding author, electronic address: mbuehler@MIT.EDU

Spider silk is one of the strongest, most extensible and toughest biological materials known, exceeding the properties of many engineered materials including steel. Silks feature a hierarchical architecture where highly organized, densely H-bonded beta-sheet nanocrystals are arranged within a semi-amorphous protein matrix consisting of 3_1-helices and beta-turn protein structures. By using a bottom-up molecular-based mesoscale model that bridges the scales from Angstroms to hundreds of nanometers, here we show that the specific combination of a crystalline phase and a semi-amorphous matrix is crucial for the unique properties of silks. Specifically, our results reveal that the superior mechanical properties of spider silk can be explained solely by structural effects, where the geometric confinement of beta-sheet nanocrystals combined with highly extensible semi-amorphous domains with a large hidden length is the key to reach great strength and great toughness, despite the

dominance of mechanically inferior chemical interactions such as H-bonding. Our model directly shows that semi-amorphous regions unravel first when silk is being stretched, leading to the large extensibility of silk. Conversely, the large-deformation mechanical properties and ultimate tensile strength of silk is controlled by the strength of beta-sheet nanocrystals, which is directly related to their size, where small beta-sheet nanocrystals are crucial to reach outstanding levels of strength and toughness. Our model agrees well with observations in recent experiments, where it was shown that a significant change in the strength and toughness can be achieved solely by tuning the size of beta-sheet nanocrystals. Our findings unveil the material design strategy that enables silks to achieve superior material performance despite simple and inferior constituents, resulting in a new paradigm in materials design where enhanced functionality is not achieved using complex building blocks, but rather through the utilization of simple repetitive constitutive elements arranged in hierarchical structures.

Submitted to: *Nature Precedings*

Introduction

Spider silk is a strong and tough fibrous biological protein material with a hierarchical structure (Fig. 1a) that has evolved to fulfill multiple functions of efficiently storing and dissipating mechanical energy [1-3], making it one of the toughest and most versatile materials known [2, 4]. Spiders take advantage of these features when using silk threads to support their own weight and to absorb kinetic energy to capture prey [1]. Silk has been utilized in various technological fields including parachutes, medical sutures, and more recently, tissue regeneration and many other biomedical applications [5].

Experimental and computational investigations of the structure of silks at the nanoscale revealed that there exist two fundamental structural constituents in silks, highly organized anti-parallel beta-sheet nanocrystals and a semi-amorphous phase that consists of less orderly protein structures (Fig. 1a) [6-8]. Thereby, the anti-parallel beta-sheet nanocrystals [9-12] play a key role in defining the mechanical properties as they provide stiff orderly cross-linking domains embedded in a semi-amorphous matrix that consists of less orderly beta-structures, 3_1 helices and beta-turns [6, 13, 14]. Similar to their role in other mechanical proteins [15-21], it has been hypothesized that H-bond arrays in beta-sheet nanocrystals reinforce the polymeric network under mechanical stretch, by forming interlocking regions that transfer the load between chains [13, 22]. In particular,

Termonia's pioneering empirical two-phase model based on experimental data has been instrumental in explaining the importance of the ratio and size of crystalline and semi-amorphous domains, at a time when large-scale atomistic simulations of spider silk constituents were impossible due to the lack of suitable force fields and computational resources [22]. More recently, macroscale experiments demonstrated that when the size of beta-sheet nanocrystals is reduced by moderating the reeling speed or by infiltrating, silk displays enhanced toughness and greater ultimate strength [22-24], exceeding that of steel and other engineered materials.

However, despite progress in experimental, theoretical and computational studies, thus far no model exists to that enables a rigorous understanding of the role of the two fundamental constituents of silks at the intermediate "composite" level (*i.e.,* the silk fibril nanostructure as shown in Fig. 1a). This progress has partly been hindered due to a lack of appropriate atomistic models of silks, and a lack of a thorough understanding of the mechanical behavior of silk's constituents at the nanoscale. Both issues have recently been addressed through protein structure identification methods and large-scale molecular simulation studies, where the molecular structure and mechanical signature of the two key constituents of silks has been identified [9, 25, 26]. As a result, we are now in a position to understand the fundamentals of the origin of silk's unique material properties directly from an atomistic level without the need to introduce experimental parameters, an issue that will be addressed in this article. The aim of this work is to utilize key material and structural parameters from atomistic calculations on dragline silk constituents and to develop a fundamental understanding of silk's exceptional performance by linking the molecular structure and mechanisms to its larger-scale mechanical behavior at scales of hundreds of nanometers.

Results and discussion

To provide a fundamental description of spider silk mechanics from a bottom-up perspective, and to elucidate the design strategy behind the making of silks, here we use a simple coarse-grained model whose parameters are directly informed from atomistic simulation results. The model setup is depicted in Fig. 1b, showing how a simple combination of beta-sheet nanocrystals as well as semi-amorphous regions is modeled by two nonlinear springs in serial arrangement to represent a unit cell of the silk two-phase nanostructure, reflecting the geometry of silk's nanostructure shown in Fig. 1a. Each constituent has a mechanical signature informed from full atomistic simulation [9, 25, 26] as shown in Fig. 2 (details on the model development and setup see Materials and Methods). This model, albeit extremely simple, is capable of describing the key features of the nanomechanics of spider silk, without the introduction of any experimental parameters.

We now apply the model to simulate the mechanical deformation of silk according to the tensile loading condition shown in the inlay of Fig. 3a, focusing first on the system with a beta-sheet nanocrystal size of 3 nm that reflects the size found in natural silks. We find that the resulting stress-strain curves display the characteristic shape observed in silks, that is, it displays an early yield point, leading to a significant softening followed by a severe stiffening effect. A detailed analysis reveals four distinct regimes of deformation, where each of them is associated with specific molecular-level mechanics as shown in Fig. 4a-b (the plots shown in Fig. 4 depict an analysis of the mechanisms of deformation as a function of increasing strain; where the deformation carried by beta-sheet nanocrystal and semi-amorphous regions is shown as a function of the total deformation [Fig. 4a,c] and as a function of their initial length [Fig. 4b,d]). The initial regime is characterized by a relatively high tangent modulus (1.07 GPa) owing to the homogeneous stretching of semi-amorphous regions that are rich in hydrogen bonding in the form of 3_1-helices and beta-turns [1, 6, 22].

The onset of rupture of the hydrogen bonds in the semi-amorphous domains leads to yielding at strain values of around 13%, evident from a sudden drop in the tangent stiffness. The tangent modulus of this softer regime is much lower, around 0.4 GPa. During this plateau regime, protein chains in the semi-amorphous region gradually align along the pulling direction [23, 27], a mechanism that is mediated by the significant hidden length of polypeptide stored in this geometry. At a strain value of 48%, the stress-strain curve enters a high-stiffness regime (with a much higher tangent stiffness of around 10 GPa). At this point, the semi-amorphous region has been completely stretched out and the beta-sheet nanocrystals begin to sustain larger strains.

The overall analysis of this data shows that beta-sheet nanocrystals play a significant role in defining the mechanical behavior of silk only at high-deformation levels, while the initial behavior is mainly governed by deformation of the semi-amorphous phase. This concept has been hypothesized in earlier experimental studies, but is here for the first time shown from a molecular perspective and with a direct link to underlying molecular mechanisms.

An interesting event observed in the stress-strain plot is the brief softening regime immediately prior to failure, which occurs at around 63% strain. A detailed analysis of this phenomenon shows that this is due to the stick-slip failure mechanism of the beta-sheet nanocrystals, a mechanism first described in [9]. This final high-stress regime contributes significantly to the overall toughness as it accounts for approximately 23% of the total energy dissipated before failure. When the applied force reaches the maximum tensile strength at strain values of 66.7%, individual beta-strands

completely are completely pulled out, and failure occurs at a stress of 1,757 MPa. This maximum stress level (on the order of GPa) is in reasonable agreement with results from experimental studies [23].

We now consider a systematic variation of the beta-sheet nanocrystal size of up to 10 nm, and study its impact on the mechanical properties to quantify the dependence of the crystal size on the overall mechanical behavior. The motivation for this analysis is to validate whether earlier hypotheses that show that small changes in the crystal size translates to altogether different overall mechanical response in spider silk [9, 23]. The results of the mechanical analysis are shown in Fig. 3a, where we plot the stress-strain curves for varying beta-sheet nanocrystal sizes. The most important finding is the observation that the size of beta-sheet nanocrystals—at otherwise completely identical conditions—severely affects the mechanical response. The analysis shown in Fig. 3a clearly shows that larger-crystal systems (*i.e.* 6.5 nm and 10 nm beta-sheet nanocrystals) have a behavior that deviates significantly from the reference small-crystal case, especially at high levels of deformation. Silk fibrils with larger beta-sheet nanocrystals break at significantly lower stress values, and also show a shorter (60% and 55% strain, respectively) and much softer third regime, with a tangent modulus of 8 GPa and 5.7 GPa, respectively. The initial and intermediate regimes, however, are comparable to the case with the smallest beta-sheet nanocrystal, where the transition points and stiffness values do not vary substantially between the two systems.

Our results demonstrate that even a slight increase in beta-sheet nanocrystal size leads to a significant loss of strength and toughness of the system (Fig. 3b-c). With a value of 1,178 MPa, the 6.5 nm-crystal case shows a decrease of approximately 33% with respect to the reference system. The drop is even larger for the 10 nm-crystal case, which fails at 570 MPa, at 67% less than the reference case with the smallest (3 nm) beta-sheet nanocrystal. The drop in maximum stress and the absence of a high-stress final stick-slip regime further lead to toughness values that are considerably lower than the reference small-crystal case (see Fig. 3c). A decrease of 43% and 63% is measured for the 6.5 nm and the 10 nm case, in comparison to the toughness value for the reference small beta-sheet nanocrystal case.

Figure 4 sheds light on the detailed deformation mechanisms at different strain levels, for varying beta-sheet nanocrystal size (two sizes are selected to provide a clear comparison). The analysis reveals that the contribution of the beta-sheet nanocrystals to deformation tends to decrease significantly as the size of beta-sheet nanocrystals is increased. In the small-crystal system, beta-sheet nanocrystals start to play a significant role once the semi-amorphous region begins to stiffen

at around 50% strain, and dominates deformation when the stick-slip mechanisms of beta-sheet nanocrystal deformation is triggered (see Fig. 4a,b). In the larger-crystal case, the beta-sheet nanocrystal contribution increases more gradually (see Fig. 4d), and reaches a maximum just before the system breaks, that is, shortly after the semi-amorphous region enters the covalent hard-stretching regime. If we compare the semi-amorphous region deformation in the two cases, shown in Fig. 4b,d, we observe that the breaking point is reached earlier in large-crystal systems, when semi-amorphous regions are less stretched (around 75%, compared to 92%). This observation suggests that the change of the beta-sheet nanocrystal size prevents the material to take full advantage of the entire potential (hidden length) of the semi-amorphous regions in terms of extensibility and energy dissipation capacity.

The results of our study are overall in good agreement with experimental data, where a similar variation of the beta-sheet nanocrystal size and its impact on larger-scale mechanical properties was reported recently [23], showing a drastic drop in toughness when beta-sheet nanocrystal size increases (in experiment this is achieved via a change of the reeling speed). We note, however, that the strain values in the three systems we investigated here are higher than those found in experimental studies (between 40% and 60%). This phenomenon can be explained based on two points. First, in our model we consider an ideal and rather simplified structure that completely lacks the statistical variability and structural defects. This generally results in enhanced strength and extensibility in comparison to experimental results. Second, it must be underlined that physiologically spun silks (*i.e.,* the small-crystal case) undergo a substantial pre-stretching at the orifice [23, 28]. However, the current model does not include this effect and consequently, we expect an overestimation of the stretching capacity. Future models could directly include variability of structure and defects in silk, and model the effect of pre-stretching to allow for a better comparison with experimental data (this could, for example, be achieved by the development of a two/three-dimensional model of silk fibrils).

Conclusions

The most important finding of our study is that it has revealed the mechanistic interplay of the two constitutive phases in silks, semi-amorphous regions and highly organized beta-sheet nanocrystals, and the effect of structural changes on the overall mechanical behavior of silks. We find that semi-amorphous regions unravel first when silk is being stretched, leading to the large extensibility of silk. Conversely, the large-deformation mechanical properties and ultimate tensile strength of silk is controlled by the strength of beta-sheet nanocrystals, which is directly related to their size. An

important discovery is that small beta-sheet nanocrystals are crucial to reach outstanding levels of strength and toughness, as shown clearly in Figs. 3 and 4.

Our results further show that the severe change of the mechanical properties of spider silk under relatively small variations of the size of beta-sheet nanocrystals can be explained solely based on structural effects (Fig. 3). Our results show that the confinement of beta-sheet nanocrystals to the nanoscale is essential for the superior mechanical properties of silks, as this is crucial to reach high extensibility and high levels of stress. Our findings also relate the characteristic yielding point in the stress-strain curve, observed universally for many silks, to the onset of failure of semi-amorphous regions when H-bonded 3_1-helices and beta-turns begin to rupture (see Fig. 2a). Small-crystal systems guarantee the required cross-linking strength that is necessary for the semi-amorphous domains to fully extend and to enter a high-stiffness covalent regime when beta-sheet nanocrystals are being stretched and eventually fail. The resulting capacity to sustain large tensile force as well as extension enhances the strength and energy dissipation ability of the material.

Our findings have impact beyond our understanding of silk mechanics, as they show that by solely controlling the structure at the nanoscale, a tailoring of material properties at the microscale is possible without the need to introduce new material constituents. This could provide us with a powerful alternative to the traditional engineering top-down approach of shaping materials to obtain specific properties. Thereby, the application of our findings to the design of synthetic materials could provide us with new material concepts based on inexpensive, abundant constituents and facilitate the development of effective cross-linking domains in other materials [29]. Technologically, we are not limited by "simple" natural building blocks such as amino acids. Therefore, the incorporation and transfer of the materials design strategies identified here into synthetic materials could result in materials with significantly better performance, and much higher levels of strength and toughness while reaching similar levels of extensibility. The incorporation of mutability concepts could be used to design materials whose mechanical properties can be controlled by external cues such as humidity [30-32], temperature, pH, magnetic or electric fields, by providing a strategy to control the nanostructure of the material.

Materials and Methods

Molecular model

A multiscale computational bottom-up investigation of spider silk, the approach employed in this work, is a powerful tool to understand its mechanical properties from a fundamental perspective. At

length-scales on the order of hundreds of nanometers, spider silk appears as an entanglement of polypeptide chains, with two distinct domains that consist of (1) a semi-amorphous region [8, 33] and (2) a highly-ordered crystalline domain [22]. We model the silk constitutive unit as a serial arrangement of these two domains, namely a crystalline beta-sheet region and a semi-amorphous domain as shown in Fig. 1c. The structure and mechanical behavior of these domains has been previously explored by atomistic simulation [25, 26].

A system made up of a series of two serial springs is a simple, yet powerful way to link nanostructural features and associated mechanical signature to the aggregate mechanical behavior at the silk fibril scale. The serial spring assumption is reasonable at the nanoscale since in the sequence of spider silk, crystalline domains are followed immediately by the glycine-rich repeats that form the semi-amorphous regions, forming a serial constitutive unit that is the fundamental building block of more complex hierarchies [34]. An extension of the model to a hierarchical arrangement of springs is trivial and could be explored in future studies. Preliminary simulations based on a two-dimensional model confirm that the mechanical properties and deformation mechanisms (as well as the sensitivity of the properties with respect to the size of beta-sheet nanocrystals) remain unaltered. We note that since the basis of the model is atomistic simulation, the (multi-linear) spring constants developed take into account the effects of solvent and molecular friction directly, and additional parameters for viscosity and other effects are not considered in this work.

Molecular model parameter identification

We approximate the stress-strain behavior of the constituting phases under tensile loading with a multi-linear model, as it has successfully been done in earlier studies of fracture [35, 36]. The constitutive relationship of the two domains in silk, derived from molecular dynamics simulations, is highly non-linear [25, 26]. It is approximated here with a multi-linear function, where different spring constants are used to describe the strain dependent effective stiffness of the protein domains.

The stiffness of the system under tensile stretch is given by a series of two springs and corresponds to

$$k_{\mathrm{T}} = k_{1i} k_{2i} / (k_{1i} + k_{2i}) \,, \qquad (1)$$

where k_{1i} and k_{2i} are the strain-dependent spring constants of semi-amorphous and crystalline domains, respectively. This results in the following expression for the force of the system as a function of deformation:

$$F_{\mathrm{T}} = k_{\mathrm{T}} \Delta L_{\mathrm{T}}, \tag{2}$$

where the total deformation is $\Delta L_{\mathrm{T}} = \Delta L_1 + \Delta L_2$, in which case ΔL_1 and ΔL_2 are the deformations of the semi-amorphous and beta-sheet nanocrystal domains, respectively. The parameters ΔL_i are defined as

$$\Delta L_i = r_{x,i} - r_{0,i}, \tag{3}$$

where $r_{x,i}$, $r_{0,i}$ are the length of the domains at a given strain, and their initial length, respectively. The following sections explain how the spring constants of the semi-amorphous and beta-sheet nanocrystal domains are obtained and implemented in the model.

Semi-amorphous region

Atomistic simulations of the mechanical properties of the semi-amorphous region of spider silk have been performed in earlier studies [25, 26]. A representative volume element containing 15 polypeptide chains is considered in deriving the constitutive mechanical law, in order to obtain good statistics and an accurate account of the secondary structure distribution of the domain. The effective force-extension behavior derived from the large molecular assembly is then normalized for the force, area and length per single polypeptide chain, to develop an appropriate constitutive law. The length of the amorphous domain is taken here as 60 Å based on the atomistic simulation model geometry. The results from these analyses are used directly to determine the parameters of the present coarse-grained model representing a single amorphous domain and a single beta-sheet nanocrystal. These simulations revealed a characteristic three-stage deformation pattern, where an initial stiff regime is followed by a yielding point and a long plateau, and eventual significant stiffening as the polypeptide's backbone is being stretched [25, 26]. This behavior is associated to the presence and the breaking of secondary structures such as 3_1-helices and beta-turns, which is rich in intra-chain and inter-chain hydrogen bonding [1, 6, 22]. At larger strains, the structure enters a final high-stiffness regime, characterized by the stretching of covalent bonds along the protein backbone.

Values for the stiffness of the three different regimes of the semi-amorphous domain are extracted from atomistic simulation data [25, 26]. By fitting the simulation curve with a tri-linear function, we obtain the following regimes of stiffness as a function of deformation:

$$k = \begin{cases} k_{11} & \text{if } \Delta L_1 < \Delta L_{11} \\ k_{12} & \text{if } \Delta L_{11} \le \Delta L_1 \le \Delta L_{12} \\ k_{13} & \text{if } \Delta L_1 > \Delta L_{12} \end{cases} \quad (4)$$

where the values for k_{1i}, as well as the transition deformations ΔL_{11} and ΔL_{12} are summarized in Table 1. The resulting force-deformation law is shown in Fig. 2a.

Beta-sheet nanocrystals

The beta-sheet nanocrystal is also modeled as a nonlinear spring, where the force-displacement characteristic is informed from atomistic simulation results [9, 25, 26, 37, 38]. We approximate the beta-sheet nanocrystal dimension in the fibril direction to be 30 Å for all beta-sheet nanocrystal sizes (since it is defined by a fixed number of alanine residues in the beta-strand length direction that does not change). From atomistic simulations [9], we found that the properties of the beta-sheet nanocrystals vary as a function of crystal size, where small crystals are stiffer, dissipate more energy through a stick-slip mechanism and fail at higher force. Here we consider the effect of the variation of the size of beta-sheet nanocrystals on the mechanical behavior, by scaling the stiffness, strength and energy dissipation capacity of the beta-sheet nanocrystals according to size-effects observed in atomistic simulations.

In this regard, beta-sheet nanocrystals of different size are prescribed distinct mechanical features [39-41] in this model. In particular, we consider a final stick-slip regime, which is observed only in the small-crystal case (3 nm), whose stiffness is modeled as follows:

$$k = \begin{cases} k_{21} & \text{if } \Delta L_2 < \Delta L_{21} \\ k_{22} & \text{if } \Delta L_2 \ge \Delta L_{21} \end{cases} \quad (5)$$

where ΔL_{21} is the beta-sheet nanocrystal transition point (as a function of deformation) as defined in Table 2 and shown in Fig. 2b. In this sense, the crystal behavior is elastic-plastic, to take into account the additional energy dissipated by the stick-slip behavior. In the case of large crystals, the spring constant is the same over the whole regime of deformations and the mechanical behavior is elastic and brittle until rupture. In all cases, the force applied to the system drops to zero when

$\Delta L_2 > \Delta L_{22}$, that is, when the maximum strength is reached and the crystal breaks. The spring constants are calculated by dividing the maximum tensile strength by the softening deformation for the 3 nm case, and by the breaking point for the large-crystal cases. The second softer regime for the small-crystal case is assumed to feature a constant stiffness equal to 1% of the initial one, approximating the stick-slip behavior observed in atomistic simulations [9]. The calculation of the breaking point is done by maintaining the dissipated-energy proportion between beta-sheet nanocrystals of different size. Explicit simulations suggest that a 3 nm crystal is approximately three times tougher than a 6.5 nm-crystal. In the context of the bilinear spring model [9], this gives a breaking point value of 5.8 Å. We note that the atomistic calculations on strength and effective stiffness are based on the pullout force required to separate a single strand from the crystal, to be consistent with the normalization for a single polypeptide strand.

The ratio of the maximum tensile strength between beta-sheet nanocrystals of different size [9] is derived directly from atomistic simulation for the 3 nm and 6.5 nm beta-sheet nanocrystals [9], while it is extrapolated for the 10 nm case. To be consistent with the force values of the semi-amorphous domain, the maximum strength is directly calculated from simulations in implicit solvent for a 3 nm-crystal system; and the large beta-sheet nanocrystal strengths are then determined using the strength ratio from explicit simulations. The softening point for the 3 nm beta-sheet nanocrystal is extracted from explicit simulation results, as well as the breaking point for the 6.5 nm beta-sheet nanocrystal. In the 10 nm case, the breaking point is instead assumed to be the same as the 6.5 nm case, given the fact that with increasing beta-sheet nanocrystal dimension the breaking point does not vary significantly as shown in [9].

Calculation of stress

Stress values are calculated by considering a constant diameter of 5 Å along the whole system length and for the three cases of beta-sheet nanocrystal size, such that $\sigma = F/A$, where σ is the computed stress, F is force per chain and A is the area of a chain. This cross-sectional area is is an approximation for the effective area of a single silk polypeptide chain. Accordingly, all other calculations have been normalized for a single-chain system for consistency.

Computing technique

The MATLAB script provided in Supplementary information is used for calculating the stress-strain behavior of the serial spring model discussed in this work. Strain is applied at constant steps to the

overall structure and the deformation on single elements is computed. Mechanical toughness is calculated measuring the area under the force-extension curve (until structural failure) by means of a trapezoidal numerical integration. Further data post-processing is performed using additional MATLAB scripts.

Acknowledgements

This work was supported by the Office of Naval Research (N00014-08-1-00844). Support from the MIT-Italy program (MITOR) is greatly acknowledged. Additional support from the National Science Foundation (CMMI-0642545 and MRSEC DMR-0819762), Army Research Office (W911NF-06-1-0291), DARPA (HR0011-08-1-0067) and the MIT Energy Initiative is acknowledged. All simulations have been carried out at MIT's Laboratory for Atomistic and Molecular Mechanics.

Author contributions

A.N., S.K., N.P., A.R., and M.J.B. designed the research and analyzed the results. A.N. and S.K. carried out the simulations. A.N., S.K. and M.J.B. wrote the paper.

References

1. Porter, D., F. Vollrath, and Z. Shao, *Predicting the mechanical properties of spider silk as a model nanostructured polymer.* The European Physical Journal E: Soft Matter and Biological Physics, 2005. **16**(2): p. 199-206.
2. Vollrath, F. and D.P. Knight, *Liquid crystalline spinning of spider silk.* Nature, 2001. **410**(6828): p. 541-548.
3. Rammensee, S., et al., *Assembly mechanism of recombinant spider silk proteins.* Proceedings of the National Academy of Sciences of the United States of America, 2008. **105**(18): p. 6590-6595.
4. Shao, Z.Z. and F. Vollrath, *Materials: Surprising strength of silkworm silk.* Nature, 2002. **418**(6899): p. 741-741.
5. Vepari, C. and D.L. Kaplan, *Silk as a biomaterial.* Progress in Polymer Science, 2007. **32**(8-9): p. 991-1007.
6. van Beek, J.D., et al., *The molecular structure of spider dragline silk: Folding and orientation of the protein backbone.* Proceedings of the National Academy of Sciences of the United States of America, 2002. **99**(16): p. 10266-10271.
7. Lefevre, T., M.E. Rousseau, and M. Pezolet, *Protein secondary structure and orientation in silk as revealed by Raman spectromicroscopy.* Biophysical Journal, 2007. **92**(8): p. 2885-2895.

8. Kummerlen, J., et al., *Local structure in spider dragline silk investigated by two-dimensional spin-diffusion nuclear magnetic resonance.* Macromolecules, 1996. **29**(8): p. 2920-2928.
9. Keten, S., et al., *Nanoconfinement controls stiffness, strength and mechanical toughness of [beta]-sheet crystals in silk.* Nat Mater, 2010. **9**(4): p. 359-367.
10. Gao, H.J., et al., *Materials become insensitive to flaws at nanoscale: Lessons from nature.* Proceedings of the National Academy of Sciences of the United States of America, 2003. **100**(10): p. 5597-5600.
11. Fossey, S.A., et al., *Conformational Energy Studies of Beta-Sheets of Model Silk Fibroin Peptides .1. Sheets of Poly(Ala-Gly) Chains.* Biopolymers, 1991. **31**(13): p. 1529-1541.
12. Xiao, S.B., et al., *Mechanical Response of Silk Crystalline Units from Force-Distribution Analysis.* Biophysical Journal, 2009. **96**(10): p. 3997-4005.
13. Hayashi, C.Y., N.H. Shipley, and R.V. Lewis, *Hypotheses that correlate the sequence, structure, and mechanical properties of spider silk proteins.* International Journal of Biological Macromolecules, 1999. **24**(2-3): p. 271-275.
14. Grubb, D.T. and L.W. Jelinski, *Fiber morphology of spider silk: The effects of tensile deformation.* Macromolecules, 1997. **30**(10): p. 2860-2867.
15. Rief, M., et al., *Reversible unfolding of individual titin immunoglobulin domains by AFM.* Science, 1997. **276**(5315): p. 1109-1112.
16. Lee, E.H., et al., *Mechanical strength of the titin Z1Z2-telethonin complex.* Structure (London, England : 1993), 2006. **14**(3): p. 497-509.
17. Marszalek, P.E., et al., *Mechanical unfolding intermediates in titin modules.* Nature, 1999. **402**(6757): p. 100-103.
18. Brockwell, D.J., et al., *Pulling geometry defines the mechanical resistance of a beta-sheet protein.* Nature structural biology, 2003. **10**(9): p. 731-737.
19. Eom, K., et al., *Relationship between the mechanical properties and topology of cross-linked polymer molecules: Parallel strands maximize the strength of model polymers and protein domains.* Journal of Physical Chemistry B, 2003. **107**(34): p. 8730-8733.
20. Sulkowska, J.I. and M. Cieplak, *Mechanical stretching of proteins - a theoretical survey of the Protein Data Bank.* Journal of Physics-Condensed Matter, 2007. **19**(28): p. -.
21. Buehler, M.J. and Y.C. Yung, *Deformation and failure of protein materials in physiologically extreme conditions and disease.* Nature Materials, 2009. **8**(3): p. 175-188.
22. Termonia, Y., *Molecular Modeling of Spider Silk Elasticity.* Macromolecules, 1994. **27**(25): p. 7378-7381.
23. Du, N., et al., *Design of superior spider silk: From nanostructure to mechanical properties.* Biophysical journal, 2006. **91**(12): p. 4528-4535.
24. Lee, S.M., et al., *Greatly Increased Toughness of Infiltrated Spider Silk.* Science, 2009. **324**(5926): p. 488-492.
25. Keten, S. and M.J. Buehler, *Atomistic model of the spider silk nanostructure.* Applied Physics Letters, 2010, doi:10.1063/1.3385388, URL: http://web.mit.edu/mbuehler/www/slides/APL_2010.pdf

26. Keten, S. and M.J. Buehler, *Nanostructure and molecular mechanics of dragline spider silk protein assemblies.* Journal of the Royal Society Interface. URL: http://web.mit.edu/mbuehler/www/slides/Interface_2010_d.pdf

27. Rousseau, M.E., et al., *Study of protein conformation and orientation in silkworm and spider silk fibers using Raman microspectroscopy.* Biomacromolecules, 2004. **5**(6): p. 2247-2257.

28. Papadopoulos, P., J. Sölter, and F. Kremer, *Hierarchies in the structural organization of spider silk—a quantitative model.* Colloid & Polymer Science, 2009. **287**(2): p. 231-236.

29. Knowles, T.P., et al., *Role of intermolecular forces in defining material properties of protein nanofibrils.* Science, 2007. **318**(5858): p. 1900-1903.

30. Vehoff, T., et al., *Mechanical Properties of Spider Dragline Silk: Humidity, Hysteresis, and Relaxation.* Biophysical journal, 2007. **93**(12): p. 4425-4432.

31. Vollrath, F. and D. Porter, *Spider silk as archetypal protein elastomer.* Soft Matter, 2006. **2**(5): p. 377-385.

32. Porter, D. and F. Vollrath, *The role of kinetics of water and amide bonding in protein stability.* Soft Matter, 2008. **4**(2): p. 328-336.

33. Michal, C.A. and L.W. Jelinski, *Rotational-echo double-resonance in complex biopolymers: a study of Nephila clavipes dragline silk.* Journal of Biomolecular Nmr, 1998. **12**(2): p. 231-241.

34. Simmons, A.H., C.A. Michal, and L.W. Jelinski, *Molecular orientation and two-component nature of the crystalline fraction of spider dragline silk.* Science, 1996. **271**(5245): p. 84-87.

35. Buehler, M.J. and H.J. Gao, *Dynamical fracture instabilities due to local hyperelasticity at crack tips.* Nature, 2006. **439**(7074): p. 307-310.

36. Buehler, M., F. Abraham, and H. Gao, *Hyperelasticity governs dynamic fracture at a critical length scale.* NATURE, 2003. **426**(6963): p. 141-146.

37. Keten, S. and M.J. Buehler, *Geometric Confinement Governs the Rupture Strength of H-bond Assemblies at a Critical Length Scale.* Nano Lett., 2008. **8**(2): p. 743-748.

38. Keten, S. and M.J. Buehler, *Asymptotic strength limit of hydrogen bond assemblies in proteins at vanishing pulling rates.* Physical Review Letters, 2008.

39. Philip, M.C., et al., *Mechanical and thermal properties of dragline silk from the spider <I>Nephila clavipes</I>*. Polymers for Advanced Technologies, 1994. **5**(8): p. 401-410.

40. Oroudjev, E., et al., *Segmented nanofibers of spider dragline silk: Atomic force microscopy and single-molecule force spectroscopy.* Proceedings of the National Academy of Sciences, 2002. **99**(90002): p. 6460-6465.

41. Krasnov, I., et al., *Mechanical properties of silk: Interplay of deformation on macroscopic and molecular length scales.* Physical Review Letters, 2008. **100**(4): p. -.

Tables and table legends

Table 1 | Model parameters for the semi-amorphous region in the mesoscale model.

Model parameter	**Value**
k_{11} (pN/Å) – Initial regime	9.9
k_{12} (pN/Å) – Intermediate regime	3.96
k_{13} (pN/Å) – Final regime	103.84
ΔL_{11} (Å) – First transition point	12.0
ΔL_{12} (Å) – Second transition point	43.8

Table 2 | Model parameters for the beta-sheet nanocrystal in the mesoscale model.

Model parameter	Beta-sheet nanocrystal size		
	3 nm crystal	**6.5 nm crystal**	**10 nm crystal**
k_{21} (pN/Å) – Beta-sheet nanocrystal initial stiffness	576	205.5	99.5
k_{22} (pN/Å) – Second-regime stiffness	5.76	N/A	N/A
ΔL_{21} (Å) – Softening point	2.36	N/A	N/A
ΔL_{22} (Å) – Breaking point	5.8	4.5	4.5
F_{max} (pN) – Maximum tensile strength	1,360	925	448

Figures and figure captions

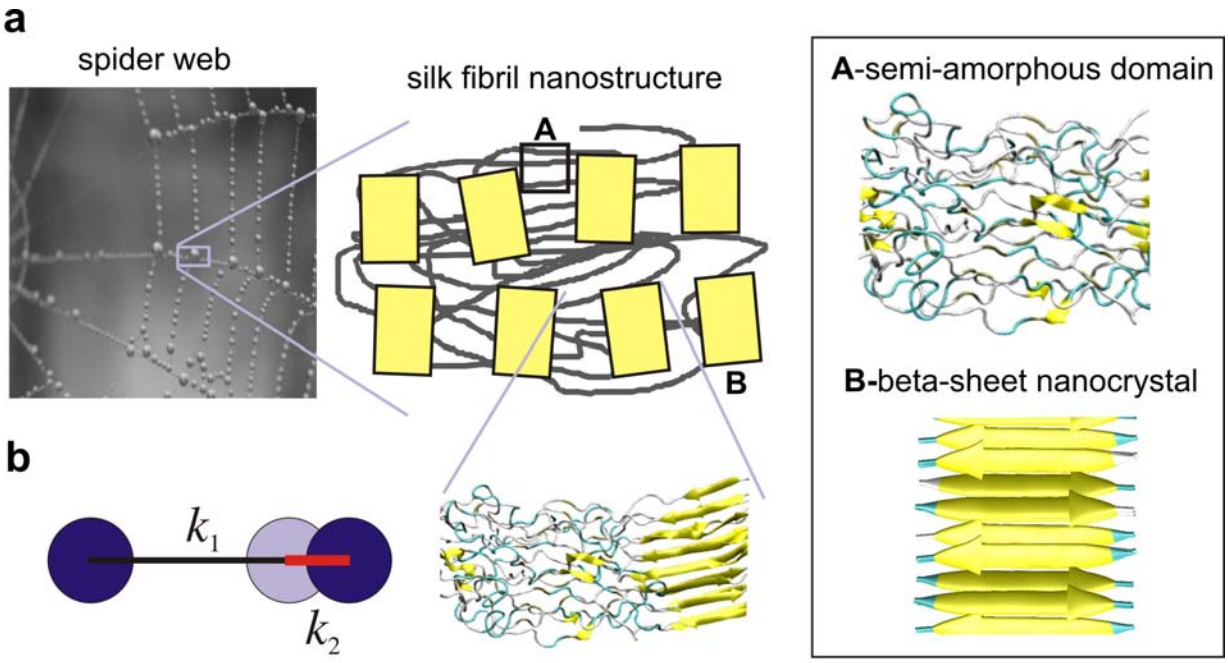

Figure 1 | Hierarchical structure of spider silk and model formulation. a, Hierarchical structure of spider silk. The nanostructure of silk fibrils consists of two major constituents, a semi-amorphous region (see inlay, **A**) and beta-sheet nanocrystals (see inlay, **B**). The focus of this study is the mesoscale level, where beta-sheet nanocrystals are embedded in a soft matrix. **b**, Representation of a spider silk mesoscale structure based on the coarse-grained model. The model is defined by a combination of a crystalline and a semi-amorphous region and mimics silk's nanostructure as shown in the inlay.

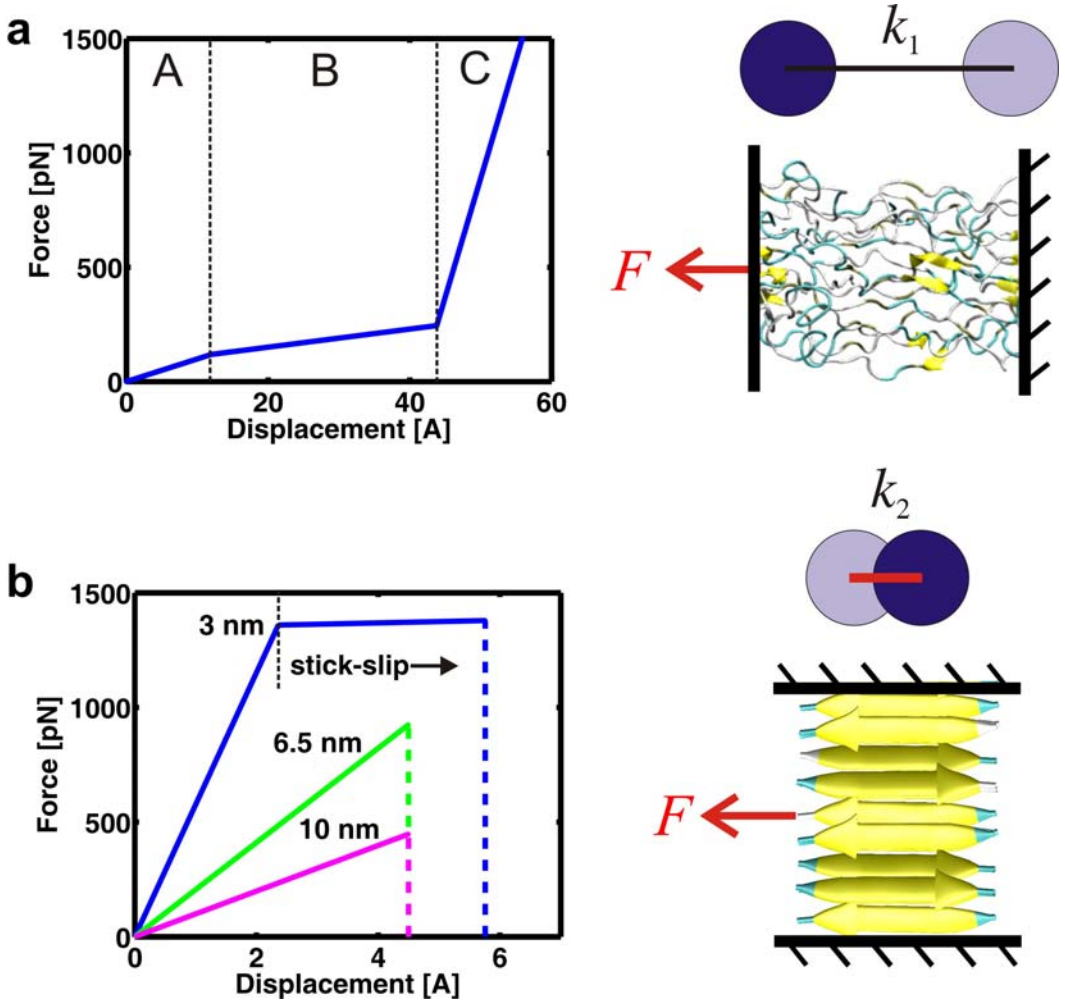

Figure 2 | Constitutive behavior of the two elements represented in the coarse-grained model of silk (obtained from full atomistic molecular dynamics simulation results as reported in [9, 25, 26]). **a**, Mechanical behavior of the glycine rich semi-amorphous domain as reported in [26], consisting of three regimes (A: homogeneous stretching of the protein structure, B: onset of yielding and unraveling of the semi-amorphous domains via the breaking of H-bonds, C: stretching of protein backbone). **b**, Mechanical behavior of beta-sheet nanocrystals under lateral loading. The smallest beta-sheet nanocrystal size shows the characteristic stick-slip phenomenon due to repeated breaking and reformation of H-bonds (modeled here as an elastic-plastic yielding behavior). Larger beta-sheet nanocrystals (>3 nm) show a more brittle and at the same time weaker and softer mechanical behavior as shown in [9]).

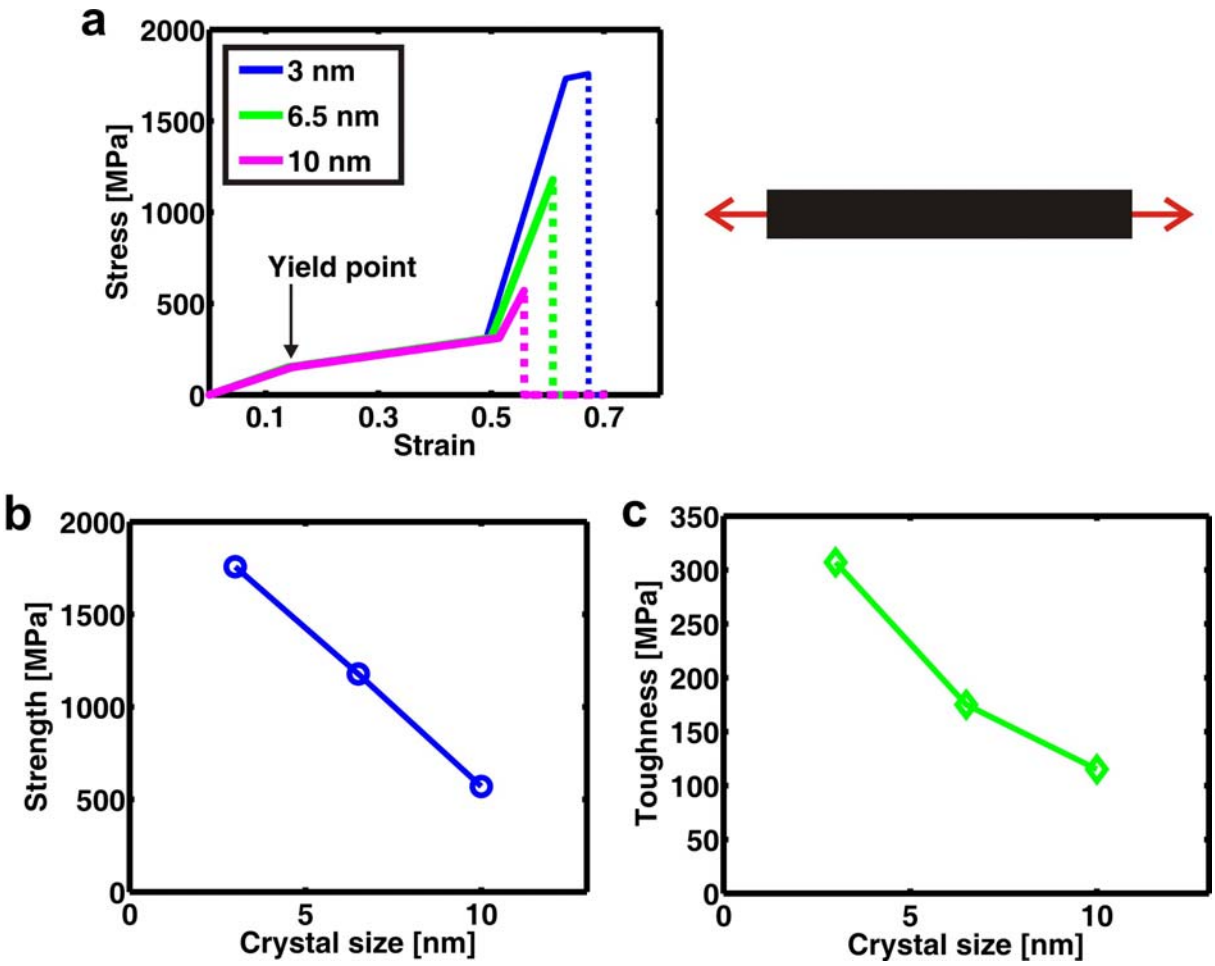

Figure 3 | Stress-strain response of a silk fibril under tensile loading, for varying beta-sheet nanocrystal size, and analysis of strength and toughness dependence on crystal size. **a**, The plot depicts the stress-strain response of spider silk based on different beta-sheet nanocrystal sizes, ranging from 3 to 10 nm. The behavior after rupture is displayed with dotted lines. The results reveal a remarkable dependence of the stress-strain response on the beta-sheet nanocrystal size. **b**, Variation of strength with beta-sheet nanocrystal size. The plot illustrates that silk fibers employing larger beta-sheet nanocrystals have a diminished strength of 1,178 and 570 MPa for the 6.5 and 10 nm crystal cases, compared with the small-crystal (3 nm) system, which breaks at 1,757 MPa. **c**. Variation in the toughness (toughness modulus) of the silk constitutive unit as a function of beta-sheet nanocrystal size. Enhanced mechanical properties of small beta-sheet nanocrystals play a governing role in the overall behavior. An increase in the toughness (modulus) from 115 MPa to 175 MPa and 307 MPa is observed when beta-sheet nanocrystal size is reduced from 10 nm to 6.5 nm and 3 nm.

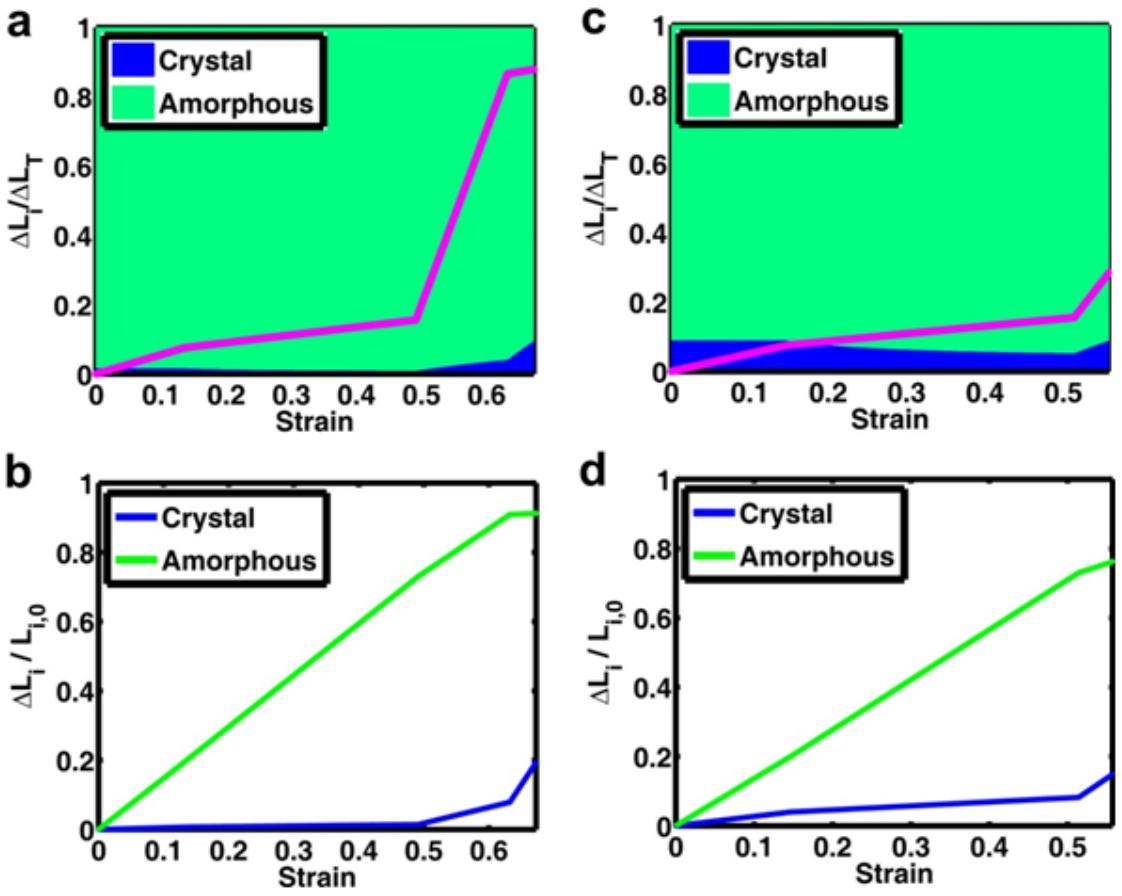

Figure 4 | Deformation mechanisms of silk constitutive elements (analysis of the smallest nanocrystal silk system [3 nm] in **a,b** and the largest crystal system in **c,d** [10 nm]). **a**, The plot shows the ratio of the beta-sheet nanocrystal and semi-amorphous region deformation over the total system deformation. Since the beta-sheet nanocrystal is much stiffer than the semi-amorphous phase, its contribution to the total deformation is initially small. A softening of the semi-amorphous phase determines an even smaller contribution for the beta-sheet nanocrystal; however, when the semi-amorphous region enters the stiff covalent regime, the beta-sheet nanocrystals deform more significantly. The final region, with a drastic drop in beta-sheet nanocrystal properties due to stick-slip phenomena, determines a noticeable increase of beta-sheet nanocrystal deformation, finally leading to failure of the system. The plot illustrates that beta-sheet nanocrystals contribute to deformation only in the final stages of stretching. **b**, Percentage of deformation of crystalline and semi-amorphous regions over their initial length. We notice that the semi-amorphous region reaches much higher deformation levels when compared to the beta-sheet nanocrystal. **c**, Since a larger beta-sheet nanocrystal is less stiff, its percentage of deformation over the total deformation is larger than in small beta-sheet nanocrystals (**a**). On the other hand, the data shown in **d** illustrates that weaker large-crystal systems prohibit the semi-amorphous region from fully extending, reducing the

energy dissipation capacity of the material. In large-crystal cases, the semi-amorphous region deforms around 80% strain, while it can reach values higher than 90% strain in the small-crystal case.

Supplementary information

MATLAB script for computing and plotting the stress-strain behavior and other mechanical properties from the coarse-grained model

```
%all lengths are in A

function monodimensional(type, color);      %type can be s (small) or l (large)
%l (large)

npoints=5000;   %how many points I have in the plot
strain=0.7;     %how much i strain the whole structure
crlength=30;    %initial length of the crystal
amlength=60;    %initial length of the amorphous region = 60 = (150-30)/2 [using MaSp2]
length=crlength+amlength;

if type=='s';
k11=576;        %all stiffnesses in pN/A
k12=0.01*k11;
r11=2.36;       %value in A
r12=5.8;

elseif type =='l';
k11=205.5;
k12=205.5;
r11=4.5;
r12=4.5;

elseif type =='xl';
k11=99.5;
k12=99.5;
r11=4.5;
r12=4.5;

end

length=crlength+amlength;

k21=9.9;
k22=3.96;
k23=103.84;
r21=0.2;    %fraction of initial length
r22=0.73;    %fraction of initial length

k2=k21;  %need to specify this for the first step of the cycle
k1=k11;

for i=1:npoints+1;
    dl(i,1)=(i-1)/npoints*strain*length;    % total deformation as a function of step

 if i==1;    %only for first step
    dl1(i,1)=k2/(k1+k2)*dl(i,1);    % deformation of each spring as a function of total
length
    dl2(i,1)=k1/(k1+k2)*dl(i,1);
 else
    dl1(i,1)=dl1(i-1,1)+k2/(k1+k2)*(dl(i,1)-dl(i-1,1));
    dl2(i,1)=dl2(i-1,1)+k1/(k1+k2)*(dl(i,1)-dl(i-1,1));
 end

    if dl2(i,1)>=r21*amlength;   %sigmoidal spring reaches 1st transition point
        if dl2(i,1)>=r22*amlength;   %sigmoidal spring reaches 2nd transition point
        k2=k23; %assigment of the new k
        else
        k2=k22;
        end
    end
```

```
    if dl1(i,1)>=r11;   %crystal spring reaches transition point
       k1=k12;
    end

    k(i,1)=k1*k2/(k1+k2); %overall system stiffness in a series of springs

    if dl1(i,1)<=r12;
        if i==1;    %particular only for first step
        f(i,1) = k(i,1)*dl(i,1);
        else
        f(i,1) = f(i-1,1)+k(i,1)*(dl(i,1)-dl(i-1,1)); %force defined as incremental value
        end
    else f(i,1)=0;  %if crystal is broken the total force goes to zero

    end
end

 %conversion to stress; diameter 5A; number in MPa:

sigma = f*1.2738853;
top=max(sigma)
maxstress=top;
location=find(sigma(:)==top);
initial=sigma(1:location);
dl5=dl(1:location);
sigma5=sigma(1:location);

plot(dl/length, sigma, [':',color], 'HandleVisibility', 'off');
hold on;
plot(dl5/length, initial, color);
set(gca, 'XTick', [0.1 0.3 0.5 0.7])

xlabel('Strain');
ylabel('Stress [MPa]');

toughness=trapz(dl5/length, sigma5)
```